

Theoretical and Numerical Analyses on Multi-Layered Ceramic Scaffold due to High Pressure for Tissue Engineering

Ming-Hwa R. Jen*, Ying-Hui Wu and Pei-Ling Guo

Department of Mechanical and Electro-Mechanical Engineering, National Sun Yat-Sen University, 80424, Taiwan.

*Corresponding, E-mail : jmhr@mail.nsysu.edu.tw

Abstract: Tissue engineering scaffolds provide temporary mechanical support for tissue regeneration and transfer global mechanical load to mechanical stimuli to cells through its architecture. The manufacturing process may cause the deformation and internal defects in multi-layered ceramic scaffold (MLCS) that results in the malfunction for tissue engineering applications. This work aims to investigate the deformation of MLCS that composed of nearly a hundred of ceramic and metal powder films interleaved and stacked due to high pressure at constant elevated temperature. On theoretical analysis, classical laminated plate theory, linear elastic assumptions and equilibrium equations were adopted. Associated with the practical process three types of boundary conditions (BCs) were used, such as all edges simple-supported, two edges simple-supported and the other two free, and four edges free. Also, two more conditions need be added, including four fixed points at corners and the elastic foundation at bottom. As for the numerical simulation the finite element method (FEM) incorporated with software ANSYS was used to obtain the displacement field of MLCS to validate the analytical prediction. Compared with the numerical results the analytical solutions were found satisfactorily acceptable, i.e., the errors were about 0.1%- 6.2% for the BCs of four edges free and four corners fixed. The errors about 0.13%- 6.15% were also acceptable for the BCs of two edges simple-supported and the others free. However, the analytical solution for the case of all the edges simple-supported did not agree with the numerical results. Finally, the proposed theoretical methodology alternatively provides an analytical method, instead of FEM and ANSYS, to analyze a nearly and over hundred layered MLCS for tissue engineering scaffolds.

[Ming-Hwa R. Jen, Ying-Hui Wu and Pei-Ling Guo. **Theoretical and Numerical Analyses on Multi-Layered Ceramic Scaffold due to High Pressure for Tissue Engineering**. Life Science Journal. 2012; 9(2):160-166] (ISSN:1097-8135). <http://www.lifesciencesite.com>. 27

Keywords: Theoretical derivation, Finite element analysis, Multi-layered ceramic scaffold, Deformation, Tissue engineering

1. Introduction

The physical characteristics required of scaffolds for tissue engineering necessitate the application of novel processing techniques for its design and fabrication. Scaffolds have been studied and fabricated using conventional techniques such as fiber bonding, solvent casting, particulate leaching, membrane lamination and melt molding [1]. In scaffold-based tissue engineering (TE) strategies, the successful regeneration of tissues and organs from matrix-producing connective tissue cells or anchorage dependent cells relies on the application of suitable substrates or scaffolds [2]. The scaffolds, built from synthetic or natural materials, serve as temporary surrogates for the native extracellular matrix (ECM). The challenge in scaffold-based TE is to construct biologic replicas in vitro such that the engineered composite becomes integrated for transplantation in vivo for the recovery of loss or malfunctioned tissues or organ. The composite should subsequently function coordinately with the rest of the body without risk of rejection or complications [3, 4].

Numerous studies have been conducted on forming

particular porous microarchitectures inside scaffolds and foam structures to obtain acceptable mechanical properties [5-7]. In addition, several groups have developed porous bone substitutes using various biomaterials including polymers, ceramics, metals and composites in an attempt to obtain biomechanical properties matching natural bone [8-10]. Bioceramics, especially calcium phosphates (CaP), are known as bone-resembling materials with excellent biocompatibility but limited mechanical strength [10-12]. Although porous ceramic materials are remarkably stiff and strong compared to polymers and composites, they are typically too brittle to resist significant cyclic loading [10, 13].

Computer-aided tissue engineering (CATE) is a newly emerging field that can be classified within three major categories: computer-aided tissue modeling, computer-aided tissue informatics and computer-aided tissue scaffold design and manufacturing [14, 15]. Application of CATE allows us to explore many novel ideas in modelling, design and fabrication of tissue scaffolds with enhanced functionality and improved interactions with cells. This is particularly useful in modeling and design of

complex bone tissue scaffolds and replacement structures that require us to simultaneously consider many biological and biophysical design requirements [16-18]. Available methods for characterization of mechanical properties of porous scaffolds and heterogeneous tissues were primarily based on using experimental approaches [19, 20], finite element numerical calculation [21-23], or effective property modeling. However, although the asymptotic homogenization theory has been well developed [24-27], the application of the theory requires a finite element implementation and the associated computational algorithm for its numerical solution.

In theoretical derivation by force method we assume that the thin plate resting on an elastic foundation [28]. For elastic foundation problem, Adewale [29] studied that the singularity function method to solve the semi-infinite orthotropic rectangular plates on a Winker-type elastic foundation. Jayachandran and Vaidyanathan [30] investigated the postbuckling response of the isotropic square thin plate subjected to biaxial compression resting on elastic foundations by the finite element method. Shen [31] presented the performances of perfect and imperfect, antisymmetrically angle-ply and symmetrically cross-ply laminated plates under combined loading and resting on Pasternak-type or softening nonlinear elastic foundations from which the results for Winkler elastic foundations were obtained as a limiting case. Horibe and Asano [32] reported the method for calculating the large deflection of a rectangular plate on an elastic foundation by the boundary integral equation method. Finally, our work is to determine the deflection of MLCS due to high pressure at constant elevated temperature with the assumption of laminated plate resting on an elastic foundation theoretically and validated numerically. The numerical simulation by FEM with software ANSYS was used to obtain the displacement field of MLCS for verification.

2 Theoretical Formulation

For simplicity, assume a homogeneous, isotropic and linearly elastic multi-layered thin plate of uniform thickness h , dimensions a , b , modulus of elasticity E and Poisson's ratio ν . The plate rests on an elastic foundation and is subjected to a biaxial inplane loading N_x , N_y and a transverse distributed load q as shown in Fig. 1. Also, the intensity of the reaction p at every point of the bottom plate is proportional to the deflection w at that point, as $p=k_w$ with k being the modulus of foundation. The deflection due to vertical pressure should be balanced by the reactive deformation of elastic foundation from the force method. Accordingly, the differential

equation for deflection in rectangular coordinates is

$$\frac{\partial^4 w}{\partial x^4} + 2 \frac{\partial^4 w}{\partial x^2 \partial y^2} + \frac{\partial^4 w}{\partial y^4} = \frac{1}{D} \left(q + N_x \frac{\partial^2 w}{\partial x^2} + N_y \frac{\partial^2 w}{\partial y^2} + 2N_{xy} \frac{\partial^2 w}{\partial x \partial y} - k_w \right) \quad (1)$$

where $D = Eh^3/[12(1-\nu^2)]$ is the flexural rigidity of the plate, E is Young's modulus, and ν Poisson's ratio.

Associated with the texts [28] and practical manufacturing process, three types of BCs were discussed, such as all edges simple-supported (S-S-S-S), two opposite edges simple-supported and the other two free (S-F-S-F), and four edges free (F-F-F-F). Also, two more conditions need be necessarily added, including four corners fixed and the bottom plate as elastic foundation.

For the case of BCs S-S-S-S as shown in Fig. 1(c), the load distributed over the surface is

$$q = \frac{16q_0}{\pi^2} \sum_{m=1,3,5,\dots} \sum_{n=1,3,5,\dots} \frac{1}{mn} \sin \frac{m\pi x}{a} \sin \frac{n\pi y}{b} \quad (2)$$

where q_0 is the intensity of the load at the center of the plate. The BCs for simple-supported edges are

$$w = 0, \quad \frac{\partial^2 w}{\partial x^2} = 0 \quad \text{for } x = 0, a \quad (3a)$$

$$w = 0, \quad \frac{\partial^2 w}{\partial y^2} = 0 \quad \text{for } y = 0, b \quad (3b)$$

To satisfy with all BCs the deflection can be expressed as

$$w = \sum_{m=1,3,5,\dots} \sum_{n=1,3,5,\dots} a_{mn} \sin \frac{m\pi x}{a} \sin \frac{n\pi y}{b} \quad (4)$$

Substituting Eqs. (2) - (4) into Eq. (1) with rearrangements [33] and neglecting the details, we receive

$$w = \frac{16q_0}{\pi^6 D} \sum_{m=1,3,5,\dots} \sum_{n=1,3,5,\dots} \frac{\sin \frac{m\pi x}{a} \sin \frac{n\pi y}{b}}{mn \left[\left(\frac{m^2}{a^2} + \frac{n^2}{b^2} \right) - \frac{N_x m^2}{D\pi^2 a^2} - \frac{N_y n^2}{D\pi^2 b^2} + \frac{k}{\pi^4 D} \right]} \quad (5)$$

Next, consider the case of S-F-S-F as illustrated in Fig. 1(d) where $0 \leq x \leq a$ and $-b/2 \leq y \leq b/2$. The BCs are

$$w = 0, \quad \frac{\partial^2 w}{\partial x^2} = 0 \quad \text{for } x = 0, a \quad (6a)$$

$$\left(\frac{\partial^2 w}{\partial y^2} + \nu \frac{\partial^2 w}{\partial x^2} \right) = 0 \quad \text{for } y = \pm \frac{b}{2} \quad (6b)$$

$$D \left[\frac{\partial^3 w}{\partial y^3} + (2-\nu) \frac{\partial^3 w}{\partial x^2 \partial y} \right] = (EI) \frac{\partial^4 w}{\partial x^4}$$

where EI is the flexural rigidity of plate. The deflection is in the form as

$$w = w_1 + w_2$$

$$\text{where } w_1 = \frac{4a^4(q - N_x - N_y)}{10^3 \pi^5 kD} \sum_{m=1,3,5,\dots} \frac{1}{m^5} \sin \frac{m\pi x}{a} \quad (7)$$

and

$$w_2 = \sum_{m=1,3,5,\dots} \frac{a^4(q - N_x - N_y)}{10^3 kD} (A_m \cosh \frac{m\pi y}{a} +$$

$$B_m \frac{m\pi y}{a} \sinh \frac{m\pi y}{a} + C_m \sinh \frac{m\pi y}{a} + D_m \frac{m\pi y}{a} \cosh \frac{m\pi y}{a} \quad (8)$$

Eqs. (7) and (8) are satisfied with the BCs. The four constants in Eq. (8) can be determined by satisfying the BCs and the symmetry. Similarly, the deflection of plate is found [33] and expressed as

$$w = \sum_{m=1,3,5,\dots} \frac{a^4(q - N_x - N_y)}{10^5 kD} \sum_{n=1,3,5,\dots} \left(\frac{4}{m^5 \pi^5} A_n \cosh \frac{m\pi y}{a} + B_m \frac{m\pi y}{a} \sinh \frac{m\pi y}{a} \right) \sin \frac{m\pi x}{a} \quad (9)$$

$$A_m = \frac{4}{m^5 \pi^5} \frac{\nu(1+\nu) \sinh \alpha_m - \nu(1-\nu) \alpha_m \cosh \alpha_m}{(3+\nu)(1-\nu) \sinh \alpha_m \cosh \alpha_m - (1-\nu)^2 \alpha_m^2} \quad (10a)$$

$$B_m = \frac{4}{m^5 \pi^5} \frac{\nu(1-\nu) \sinh \alpha_m}{(3+\nu)(1-\nu) \sinh \alpha_m \cosh \alpha_m - (1-\nu)^2 \alpha_m^2} \quad (10b)$$

where $\alpha_m = m\pi b/2a$ and $\lambda = EI/aD$

Substituting $\lambda=0$ into Eq. (10), we obtain the constants in Eq. (9) for the case of S-F-S-F.

Finally, for the case of F-F-F-F as illustrated in Fig. 1(e) where $-a/2 \leq x \leq a/2$ and $-b/2 \leq y \leq b/2$.

In such case the BCs are

$$\left(\frac{\partial^2 w}{\partial x^2} + \nu \frac{\partial^2 w}{\partial y^2} \right) = 0 \quad \text{for } x = \pm \frac{a}{2} \quad (11a)$$

$$D \left[\frac{\partial^3 w}{\partial x^3} + (2-\nu) \frac{\partial^3 w}{\partial y^2 \partial x} \right] = (EI \frac{\partial^4 w}{\partial y^4})$$

$$\left(\frac{\partial^2 w}{\partial y^2} + \nu \frac{\partial^2 w}{\partial x^2} \right) = 0 \quad \text{for } y = \pm \frac{b}{2} \quad (11b)$$

$$D \left[\frac{\partial^3 w}{\partial y^3} + (2-\nu) \frac{\partial^3 w}{\partial x^2 \partial y} \right] = (EI \frac{\partial^4 w}{\partial x^4})$$

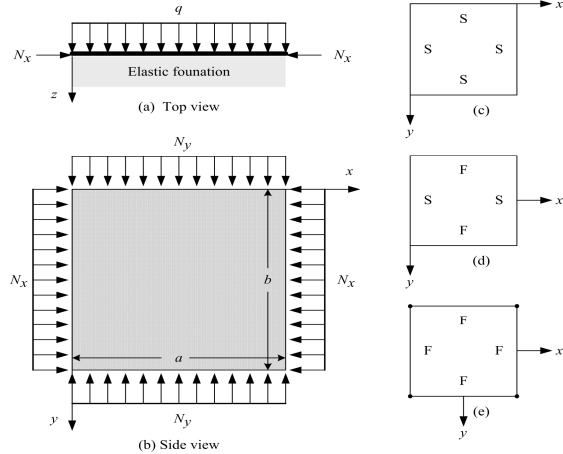
The deflection of w can be expressed as

$$w = \left\{ \frac{q}{384D(\gamma + \delta)} [\lambda(16x^4 - 24a^2x^2 + 5a^4) + \delta(16y^4 - 24b^2y^2 + 5b^4)] \right.$$

$$+ \sum A_n \cosh \frac{n\pi y}{a} \cos \frac{n\pi x}{a} + \sum B_n \cosh \frac{n\pi x}{b} \cos \frac{n\pi y}{b} + \sum C_n y \sinh \frac{n\pi y}{a} \cos \frac{n\pi x}{a} + \sum D_n \sinh \frac{n\pi x}{b} \cos \frac{n\pi y}{b} \left. \right\} \frac{D(q - N_x - N_y)}{10^5 k} \quad (12)$$

where δ/λ and A_n, \dots, D_n are some constants and $n=1,3,5,\dots$. In a particular case of $EI=0$, $n=1$, $\delta/\lambda=1$, $A_1 = B_1$, $C_1 = D_1$, and $\lambda = EI/aD$, we have a square plate carrying a biaxial inplane loading and a uniform pressure and supported only at the corners. After calculations the constants, $B_1 = 5479.3868$ and $D_1 = -33354.3362$, are obtained [33].

From the above-mentioned investigation, the deflection w associated with three BCs of MLCS can be accomplished.



Note: S: simple-supported edge, F: free edge
Figure 1. Scheme of MLCS under vertical and lateral pressures on elastic foundation at various boundary conditions

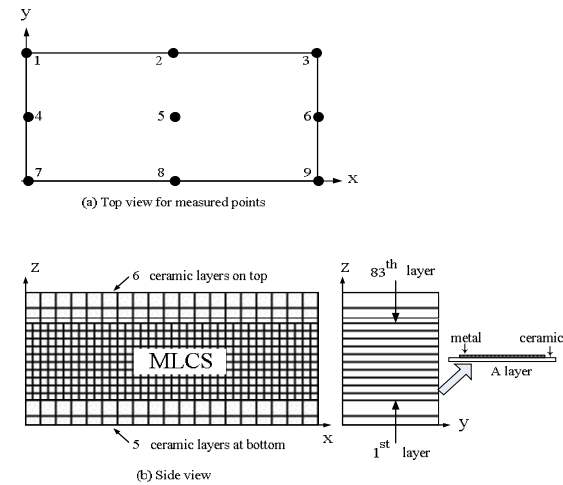


Figure 2. The geometry of 83-layered MLCS

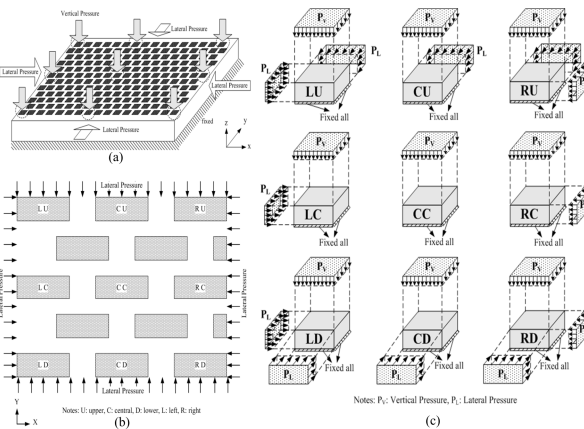


Figure 3. Scheme of MLCS under vertical and lateral pressures (a) side view (b) top view (c) loading positions for nine locations in MLCS

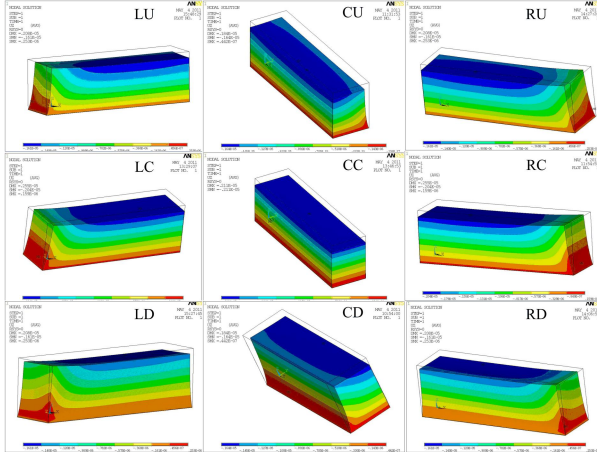


Figure 4. The displacements of u , v and w subjected to uniformly vertical pressure by loading positions for nine locations in MLCS

3 Numerical Simulation

Figure 2 shows the geometry of MLCS, and the dimensions of a ceramic film are $1.368\text{mm} \times 0.345\text{mm} \times 2.25\mu\text{m}$ ($L \times W \times T$), and a metal powder film $1.188\text{mm} \times 0.175\text{mm} \times 1.6\mu\text{m}$, respectively. The Young's moduli of both films, such as $E_{\text{BaTiO}_3} = 3.53\text{GPa}$ and $E_{\text{Ni}} = 4.09\text{GPa}$, were obtained by nanoindentation testing^[33], however, the Poisson's ratio and coefficient of thermal expansion were adopted from^[35], 0.33 for ceramic and 0.26 for metal powder films, and the coefficients of thermal expansion are $9.8\text{ppm}/^\circ\text{K}$ and $13.3\text{ppm}/^\circ\text{K}$, respectively. The SEM micrographs of ceramic film and printed metal powder film were also obtained^[33]. It can be observed that the grain boundary becomes more and more clear with the increase of temperature and time. That means almost no phase changes occur in the manufacturing process of MLCS.

The MLCS were subjected to high hydrostatic pressure at elevated temperature in processing. Two types of vertical loading were investigated, such as the uniform pressure and slant pressure of 1° inclination. The vertical pressures include 8000, 10000, 12000, 16000 and 20000 psi . Also two lateral pressures were added, such as the uniform and linearly distributed pressures. The temperature was kept at constant of 85°C . The BCs include fixed at bottom and other sides free as shown in Figure 3.

For Simplicity, the sample is reasonably assumed elastic, isotropic and homogeneous. The friction and gap between layers can be ignored. A pre-study was

performed by using software, ANSYS. Eight-node solid element (Solid 45) and twenty-node solid element (Solid 95) were used^[34, 35]. In order to assure the preciseness of simulation the convergence analysis was reasonably done in advance. By the results of convergence analysis, the errors at special area obtained from both coarse and refined meshes of the metal electrode were less than 0.002%. In order to observe and focus on the special zone that the mapped mesh method was properly adopted.

4 Results

In nanoindentation two test points were so close that an error of Young's modulus was found. After a series of tests of the point distances of 10, 50 and $100\mu\text{m}$, it is suggested that two test points should be at least $100\mu\text{m}$ apart. Only two load-displacement curves were deviated away, then these two unloading curves couldn't be adopted for Young's modulus calculation^[33].

The numerical results of deformations, i.e., u_x , u_y , u_z of metal electrode at the first layer(bottom), 20th, 40th, 60th, and 80th (top)layer, subjected to uniformly vertical pressure, 69MPa ($\approx 10000\text{psi}$) of practical use, were showed in Fig. 4, as an example. The results due to other pressures, such as 8000-20000 psi were omitted. Also, it is found that the deformations and stresses do not change significantly due to a 1° inclination of vertical pressure. Hence, the results of slightly inclined pressure were neglected. It needs be mentioned that the locations of maximal deformation were also marked according to Fig. 3(b).

The theoretical analysis for S-S-S-S, S-F-S-F and F-F-F-F plates subjected to uniformly vertical pressure combined with biaxial compression and resting on elastic foundations. For all cases the material properties, dimensions and uniform pressure are $E = 3.810\text{GPa}$, $\nu = 0.3$, $h = 429.55\mu\text{m}$, $a = b = 0.15\text{m}$ and $q = 69\text{MPa}$, respectively. Young's modulus E and Poisson's ratio ν are obtained by the rule of mixtures of two parts. The theoretical results of deformations, u_z , of metal electrode at the top layer, subjected to uniformly vertical pressure, 69MPa and a biaxial inplane loading for various BCs were selected and listed in Table 1. The errors of the numerical results compared with the analytical solutions were listed in Table 2.

Table 1. The deformation, u_z , of analytical solutions of the top layer subjected to uniformly vertical pressure, 69MPa by various boundary conditions

location	B. C.	Deflection of measured point (μm)								
		1	2	3	4	5	6	7	8	9
LU	S-S-S-S	0	0	0	0	0.03	0.06	0	0.05	0.09
	S-F-S-F	0	1.36	1.32	0	1.53	1.55	0	1.53	1.55
	F-F-F-F	0	1.08	1.27	0.57	1.4	1.45	0.86	1.56	1.53
LC	S-S-S-S	0	4.72	9.66	0	4.72	9.66	0	4.72	9.66
	S-F-S-F	0	1.92	1.9	0	1.92	1.9	0	1.92	1.9
	F-F-F-F	1.26	1.96	1.97	1.26	1.96	1.97	1.26	1.96	1.97
LD	S-S-S-S	0	0.05	0.11	0	0.03	0.05	0	0	0
	S-F-S-F	0	1.53	1.55	0	1.53	1.55	0	1.36	1.32
	F-F-F-F	0.99	1.63	1.57	0.49	1.36	1.42	0	1.08	1.27
CU	S-S-S-S	0	0	0	1.38	1.38	1.38	2.07	2.07	2.07
	S-F-S-F	1.37	1.37	1.37	1.56	1.56	1.56	1.56	1.56	1.56
	F-F-F-F	1.36	1.36	1.36	1.52	1.52	1.52	1.61	1.61	1.61
CC	S-S-S-S	251	251	251	251	251	251	251	251	251
	S-F-S-F	2.01	2.01	2.01	2.01	2.01	2.01	2.01	2.01	2.01
	F-F-F-F	2.01	2.01	2.01	2.01	2.01	2.01	2.01	2.01	2.01
CD	S-S-S-S	2.38	2.38	2.38	1.19	1.19	1.19	0	0	0
	S-F-S-F	1.56	1.56	1.56	1.56	1.56	1.56	1.37	1.37	1.37
	F-F-F-F	1.61	1.61	1.61	1.52	1.52	1.52	1.36	1.36	1.36
RU	S-S-S-S	0	0	0	0.06	0.03	0	0.09	0.05	0
	S-F-S-F	1.32	1.39	0	1.55	1.56	0	1.55	1.56	0
	F-F-F-F	1.27	1.11	0	1.45	1.42	0.57	1.53	1.58	0.86
RC	S-S-S-S	9.66	4.83	0	9.66	4.83	0	9.66	4.83	0
	S-F-S-F	1.9	1.96	0	1.9	1.96	0	1.9	1.96	0
	F-F-F-F	1.97	1.96	1.26	1.97	1.96	1.26	1.97	1.96	1.26
RD	S-S-S-S	0.11	0.05	0	0.05	0.03	0	0	0	0
	S-F-S-F	1.56	1.56	0	1.55	1.56	0	1.32	1.39	0
	F-F-F-F	1.57	1.65	0.99	1.42	1.38	0.49	1.27	1.11	0

Notes:

- please refer to Fig. 4(b) for positions (U: upper, C: central, D: lower, L: left, R: right)
- please refer to Fig. 3 for measured points

Table 2. The errors of compared with numerical results and analytical solutions of the top layer at various locations on S-F-S-F and F-F-F-F

location	B. C.	Error of deflection of measured point (%)								
		1	2	3	4	5	6	7	8	9
LU	S-F-S-F	--	0.48	0.57	--	1.04	2.65	--	3.83	0.51
	F-F-F-F	--	20	3	28	9.3	4.1	2.4	1.9	1.3
LC	S-F-S-F	--	1.58	2.37	--	5.08	2.81	--	1.73	2.37
	F-F-F-F	33.4	0.5	1.1	32.6	3.1	0.6	33.4	0.3	1.1
LD	S-F-S-F	--	3.8	0.53	--	4.07	6.15	--	1.55	0.57
	F-F-F-F	12.3	2.6	1.3	41	14.8	2.5	--	21.7	3
CU	S-F-S-F	4.28	0.13	4.28	5.51	0.95	1.95	1.29	5.14	1.29
	F-F-F-F	3.4	0.7	3.4	3.4	2.9	0.1	2	2	2
CC	S-F-S-F	0.74	2.5	1.74	0.3	4.62	0.3	0.74	2.63	1.74
	F-F-F-F	0.6	2.6	0.6	0.2	4.7	0.2	0.6	2.7	0.6
CD	S-F-S-F	1.31	5.13	1.31	1.97	4.22	5.53	4.28	2.24	4.28
	F-F-F-F	2	1.9	2	0.1	6.2	3.4	3.4	3.1	3.4
RU	S-F-S-F	0.6	2.5	--	2.7	2	--	0.5	2.4	--
	F-F-F-F	3	18.4	--	4.1	7	31.6	1.3	1.2	2.4
RC	S-F-S-F	2.4	0.5	--	2.8	1.7	--	2.4	0.7	--
	F-F-F-F	1.1	0.8	33.4	0.6	1.9	32.6	1.1	0.9	33.4
RD	S-F-S-F	0.5	2.4	--	6.1	1.1	--	0.6	0.3	--
	F-F-F-F	1.3	3.2	12.3	2.5	12.6	37.9	3	20.1	--

Notes:

- "--" denotes the data of the fixed edge can neglected.
- please refer to Fig. 4(b) for positions (U: upper, C: central, D: lower, L: left, R: right)
- please refer to Fig. 3 for measured points

5 Discussion

From Figure 3 it is obvious to see only the first quadrant of MLCS needs be analyzed due to the geometric symmetry, and also six locations, such as LU, CU, RU, RC, RD and CC, are considered. After simulation the largest deformation of u_x occurs at locations RC and LC, and u_y at locations CU and CD similarly, since both largest u_x and u_y look the same after a rotation 90° , i.e., they are compressed by vertical pressure of $69MPa$ and subjected to lateral pressure simultaneously. However, the largest u_z occurs at location CC with both-side lateral pressure balanced. From Figure 4 it is easily found that the deformation, u_z , of electrode films decrease as the lateral pressure number increasing, i.e., more pressure cumulatively acting on the top layer. Also, the deformations become larger at the corners of electrode because of the well-known free-edge effect.

For practical applications, both vertical pressure ($69MPa$) and lateral pressure are applied simultaneously. All the deformations, u_x , u_y and u_z , are increasing from the bottom to the top, especially the maximal values occur at the top layer.

The trends of stress and deformation fields due to other pressures, i.e., 8000, 12000, 20000psi, are similar to those results as above mentioned for $69MPa$, since our priory assumptions for both films are linear and elastic. Nevertheless, the pressure over 20000psi will crush the films, i.e., it is too high to fabricate MLCS.

The MLCS green sheets were divided into nine measure points per one region with suitably different boundary conditions. Compared with the numerical results and the analytical solutions of nine measure points were found satisfactorily acceptable. As shown in Table 2, the errors were about 0.1%- 6.2% for the boundary conditions of four edges free and four corners fixed. The errors about 0.13%- 6.15% were also acceptable for the boundary conditions of two opposite edges simple-supported and the others free. However, the analytical solutions did not agree with the numerical results for the case of all the boundary conditions simple-supported.

6 Conclusion

The deformation field in MLCS subjected to vertical and lateral pressures at high temperature were obtained by theoretical analysis and numerical simulation incorporated with FEM and ANSYS. The duration of high temperature tests were performed to assure no phase changes in both ceramic and electrode films. Also, nanoindentation tests were done to obtain the Young's modulus of both films as the input data for simulation. Finally, the concluding remarks can be summarized as follows:

- The material properties of both ceramic and

metal powder films, as the input data, were obtained by nanoindentation.

- The assurance of no phase changes of both films was confirmed by high temperature tests in advance.
- The analytical prediction of deflection and stress fields was validated by the numerical simulation of FEM and software ANSYS with very small errors.

The achieved analytical methodology can be used to multi-layered plate instead of conventional numerical methods with commercial softwares for applications of tissue engineering scaffolds.

Corresponding Author:

Prof.: Ming-Hwa R. Jen

Department of Mechanical and Electro-Mechanical Engineering, National Sun Yat-Sen University, 80424, Taiwan; E-mail: jmhr@mail.nsysu.edu.tw

References

1. Hutmacher DW. Scaffolds in tissue engineering bone and cartilage. *Biomaterials* 2000;21:2529-43.
2. Ingber DE. Mechanical, chemical determinants of tissue development. In: Lanza RP, Langer RS, Vacanti JP, editors. *Principles of tissue engineering*, 2nd ed. San Diego: Academic Press, 2000:101-10.
3. Bell E. Tissue engineering in perspective. In: Lanza RP, Langer RS, Vacanti JP, editors. *Principles of tissue engineering*. 2nd ed. San Diego: Academic Press, 2000.
4. Martins-Green M. Dynamics of cell-ECM interactions. In: Lanza RP, Langer RS, Vacanti JP, editors. *Principles of tissue engineering*, 2nd ed. San Diego: Academic Press, 2000:33-56.
5. Lin CY, Kikuchi N, Hollister SJ. A novel method for biomaterial scaffold internal architecture design to match bone elastic properties with desired porosity. *J. Biomech.* 2004;37(5):623-36.
6. Hollister J. Porous scaffold design for tissue engineering. *Nat. Mater.* 2005;4:518-24.
7. Lin ASP, Barrows TH, Cartmell SH, Guldberg RE. Microarchitectural and mechanical characterization of oriented porous polymer scaffolds. *Biomaterials* 2003;24(3):481-9.
8. Hutmacher DW. Scaffolds in tissue engineering bone and cartilage. *Biomaterials* 2000; 21(24):2529-43.
9. Ma PX, Elisseeff J, editors. *Scaffolding in tissue engineering*. Boca Raton, FL: Taylor & Francis; 2006.
10. Mistry AS, Mikos AG. *Tissue engineering*

- strategies for bone regeneration. *Adv. Biochem. Eng. Biotechnol.* 2005;94:1–22.
11. Dorozhkin SV. Bioceramics of calcium orthophosphates. *Biomaterials* 2010; 31(7):1465-85.
 12. Shi D, editor. *Introduction to biomaterials.* Singapore: World Scientific; 2006.
 13. Guilak F, Butler DL, Goldstein SA, Mooney D, editors. *Functional tissue engineering.* New York: Springer Verlag. 2004.
 14. Sun W, Lal P. Recent development on computer aided tissue engineering—a review. *Comput. Methods and Programs in Biomed.* 2002;67:85-103.
 15. Sun W, Darling A, Starly B, Nam J. Computer-aided tissue engineering: application to biomimetic modelling and design of tissue scaffolds. *Biotechnology and Appl. Biochem.* 2004;39:29-47.
 16. Currey, JD. The relationship between the stiffness and the mineral content of bone. *J. Biomech.* 1969;2:477-80.
 17. Hutmacher DW. Scaffolds in tissue engineering bone and cartilage. *Biomaterials* 2000;21:2529-43.
 18. Hollister SJ, Levy RA, Chu TW, Halloran JW, Feinberg SE. An image-based approach for designing and manufacturing craniofacial scaffolds. *Int. J. Oral Maxillofacial Surg.* 2000;29:67-71.
 19. Hing K, Best S, Bonfield W. Characterization of porous hydroxyapatite. *J. Mater. Sci.: Mater. Med.* 1999;10:135-45.
 20. Bose S, Darsell J, Hosick H, Yang L, Sarkar D, Bandyopadhyay A. Processing and characterization of porous alumina scaffolds. *J. Mater. Sci.: Mater. Med.* 2002;13:23-8.
 21. Beaupr GS, Hayes WC. Finite element analysis of a three dimensional open celled model for trabecular bone. *J. Biomech. Eng.* 1985;107:249-56.
 22. Williams JL, Lewis JL. Properties and an anisotropic model of cancellous bone from the proximal tibia epiphysis. *J. Biomech. Eng.* 1982;104:50-6.
 23. Huang BW, Kung HK, Chang KY, Hsu PK, Tseng JG. Human Cranium Dynamic Analysis. *Life Science Journal* 2009;6:15-22.
 24. Huang BW, Wang FS, Ko JY, Jhong WH, Yen KT, Tseng JG. Mechanical Stimulation Effect on Proliferation of Murine Osteoblast Cell. *Life Science Journal* 2009;7:62-7.
 25. Guedes JM. Nonlinear computational models for composite materials using homogenization. PhD Thesis, Department of Mechanical Engineering and Applied Mechanics, University of Michigan. 1990.
 26. Guedes JM, Kikuchi N. Preprocessing and postprocessing for materials based on the homogenization method with adaptive finite element methods. *Computer. Meth. Appl. Mech. Eng.* 1990;83:143-98.
 27. Gdoutos F, Dumontet H, Duvaut G, Lene F. Homogenization and damage for composite structures. *Int. J. Numer. Meth. Eng.* 1989;27:285-98.
 28. Timoshenko S, Woinowsky-Krieger S. *Theory of plates and shells.* 2nd ed., McGraw-Hill, Inc., New York, 1959:259-81.
 29. Adewale O. Application of the singularity function method to semi-infinite orthotropic rectangular plates on an elastic foundation. *Mechanical Sciences* 2001;43: 2261-79.
 30. Arul JS, Vaidyanathan CV. Post critical behaviour of biaxially compressed plates on elastic foundation. *Computer & Structures* 1995;54: 239-46.
 31. Shen HS. Postbuckling of shear deformable laminated plates under biaxial compression and lateral pressure and resting on elastic foundations. *Mechanical Sciences* 2000;42: 1171-1195.
 32. Horibe T, Asano N. Large Deflection Analysis of Rectangular Plates on Two-parameter Elastic Foundation by the Boundary Strip Method. *JSME Int. J. Series A* 2001;44:483-89.
 33. Guo PL. Analysis on the Deflection of Multilayered Ceramic Capacitors under High Temperature and Uniform Pressure, M. S. Thesis, Dep. of Mechanical and Electro-Mechanical Engineering National Sun Yat-Sen University, Kaohsiung, Taiwan, 2011.
 34. Hu HL. Reliability of Evaluation and Failure Analysis for Multilayer Ceramic Capacitors (MLCCs). M. S. Thesis, Dep. of Eng. Sci. National Cheng Kung University, Taiwan, 2006.
 35. Zahavi E. *The Finite Element Method in Machine Design,* Int. ed., Prentice Hall, Englewood Cliffs, 1992:47-51.

3/15/2012